Ultrasensitive and Broadband MoS_2 Photodetector Driven by Ferroelectrics

Xudong Wang, Peng Wang, Jianlu Wang, Weida Hu,* Xiaohao Zhou, Nan Guo, Hai Huang, Shuo Sun, Hong Shen, Tie Lin, Minghua Tang, Lei Liao, Anquan Jiang, Jinglan Sun, Xiangjian Meng, Xiaoshuang Chen, Wei Lu, and Junhao Chu*

During the past ten years, because of the unique properties of single layer graphene, 2D materials draw more and more attention for their potential applications in future nanoscale electronic/optoelectronic devices.[1–13] Molybdenum disulfide (MoS_2), consisting of layered S–Mo–S units structures bonded by van der Waals forces, has also been widely studied in recent years.[2,8,9,14–17] MoS_2 is a typical semiconductor with a band gap range from 1.2 to 1.8 eV as the thickness decreases from bulk to monolayer.[18–20] Field effect transistors based on monolayer or multilayer MoS_2 possess high current ON/OFF ratios of up to 10^7–10^8. [21–23] Owing to these special features, ultrathin MoS_2 becomes a promising candidate material for future electronic applications.

For transistors based on 2D graphene and MoS_2, traditional dielectric materials, such as SiO_2, HfO_2, and Al_2O_3, possessing linear dielectric response to an electric field, are usually selected as gate dielectrics.[1,8,14,16,17] Many interesting and meaningful physical properties have been discovered using these materials. Among these, the optoelectronic properties of a field effect transistor, especially the MoS_2 photodetector (sometimes named a phototransistor), have attracted intensive attention.[14–17] For these photodetectors, the photoresponsivity is relatively low, with the first monolayer MoS_2 phototransistors exhibiting a photoresponsivity of 7.5 mA W^{-1}.[15] The specific detectivity D^* for a photodetector, a figure of merit used to characterize performance, is a metric of detector sensitivity. Among these photodetectors, the detectivity is unfavorable for practical applications. Additionally, for these traditional photodetectors, additional gate bias (V_g) and a large drain-source bias (V_{sd}) are essential for obtaining high sensitivity. Such V_g may induce a leakage between source and gate, and the large V_{sd} leads to a significant increase in dark current between the source and drain, as well as a self-heating effect in the channel. These effects will not only cause a large power dissipation but will also seriously degrade the performance, such as low sensitivity.[24,25] In recent years, poly(vinylidene fluoride-trifluoroethylene) (P(VDF-TrFE)) ferroelectric polymer films and (lithium niobate) $LiNbO_3$ ferroelectric crystal has been used in nano electronic devices, such as nonvolatile memories.[26–31] In these devices, the function of the ferroelectric film is to tune the transport properties of the channel. However, ferroelectric materials combined with the photoelectric 2D materials have never been used for optoelectronic devices, for example, photodetectors.

In this work, the MoS_2 transistor with a ferroelectric gate is used as a photodetector, wherein the few-layer MoS_2 serves as the photosensitive semiconducting channel while the remnant polarization of P(VDF-TrFE) is employed to depress the dark current of the MoS_2 semiconducting channel. The stable remnant polarization can provide an ultrahigh local electrostatic field ($\approx 10^9$ V m^{-1} within a several nanometer scale) in the semiconductor channel which is larger than that produced by gate bias in traditional field effect transistors.[15–17] With such an ultrahigh electrostatic field, the few-layer MoS_2 channel is maintained in a fully depleted state, significantly increasing the sensitivity of the detector even at ZERO gate voltage. Based on these special properties, a photodetector with high detectivity $\approx 2.2 \times 10^{12}$ Jones and photoresponsivity up to 2570 A W^{-1} has been achieved. In addition, for the first time the photoresponse wavelengths of the ferroelectric polarization gating MoS_2 photodetector are extended from the visible to the near-infrared (0.85–1.55 μm).

A few-layer MoS_2 on a degenerately doped silicon substrate covered with a 285 nm thick silicon oxide was prepared using the Scotch tape-based mechanical exfoliation method.[2,8] The molecular configurations of MoS_2 are shown in **Figure 1**a. The source and drain chromium (Cr, 5 nm)/gold (Au, 50 nm) electrodes were prepared using the lift-off method. The following step was coating the P(VDF-TrFE) (70:30 in mol%) film as the top gate. The molecular configurations of P(VDF-TrFE)

X. Wang, P. Wang, Dr. J. Wang, Prof. W. Hu, Dr. X. Zhou, N. Guo, H. Huang, Dr. S. Sun, Dr. H. Shen, Dr. T. Lin, Prof. J. Sun, Prof. X. Meng, Prof. X. Chen, Prof. W. Lu, Prof. J. Chu
National Laboratory for Infrared Physics
Shanghai Institute of Technical Physics
Chinese Academy of Sciences
500 Yu Tian Road, Shanghai 200083, China
E-mail: jlwang@mail.sitp.ac.cn; wdhu@mail.sitp.ac.cn
X. Wang, Prof. M. Tang
School of Materials Science and Engineering
Xiangtan University
Xiangtan, Hunan 411105, China
Prof. L. Liao
Department of Physics and Key Laboratory of Artificial Micro- and Nano-Structures of Ministry of Education
Wuhan University
Wuhan 430072, China
Prof. A. Jiang
Department of Microelectronics
Fudan University
220 Handan Road, Shanghai 200433, China

DOI: 10.1002/adma.201503340

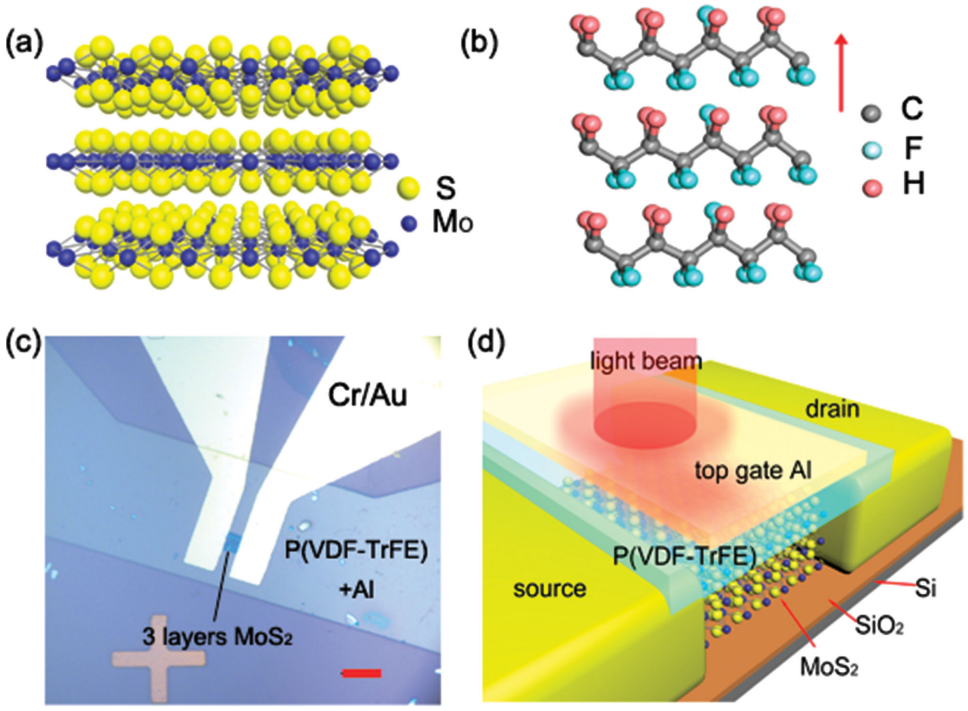

Figure 1. Fabrication and structure of few-layer MoS_2 photodetector. a) Schematic structure of triple-layer MoS_2. b) Schematic structure of P(VDF-TrFE) ferroelectric polymer. The polarization direction of the polymer is pointed out by arrow. c) Optical image of the whole device. The device is comprised of triple-layer MoS_2 with Cr/Au contract, 300 nm P(VDF-TrFE) ferroelectric polymer and semitransparent aluminum top electrode. Scale bar, 10 μm. d) 3D schematic view of the triple-layer MoS_2 photodetector with monochromatic light beam.

are shown in Figure 1b. The ferroelectric dipole direction in the P(VDF-TrFE) chain is also shown in Figure 1b. Then the ultrathin semitransparent aluminum (≈15 nm) electrodes were deposited. The thickness of the few-layer MoS_2 was confirmed by the Raman spectrum (Figure S1, Supporting Information). The peak locations of E^1_{2g} and A_{1g} are 381.32 and 404.65 cm^{-1}, respectively, and the frequency difference between E^1_{2g} and A_{1g} vibration modes is 23.27 cm^{-1}. These data correspond to a film thickness of 2.1 nm for the triple-layer MoS_2.[18,19] The optical image of the whole device based on MoS_2 and P(VDF-TrFE) is shown in Figure 1c. The 3D device structure schematic view of the ferroelectric polarization gating MoS_2 photodetector with laser beam illumination is shown in Figure 1d.

Then, the ferroelectric properties of P(VDF-TrFE) copolymer films have been characterized. A typical hysteresis loop for a P(VDF-TrFE) capacitor is shown in **Figure 2**a. The thickness of the P(VDF-TrFE) layer is 300 nm. The coercive voltage is ≈22.5 V and the remnant polarization value is 7 μC cm^{-2}. The polarization switching voltage can be reduced to ≈5 V with decreasing thickness of the ferroelectric layer.[27] Next, the transfer curves I_{sd}–V_{tg} (drain-source current I_{sd} as a function of top gate voltage V_{tg}) of the MoS_2 transistor with ferroelectric polymer were investigated at room temperature (shown in Figure 2b). The large memory window (≈25 V) in I–V curves between the voltage rise and decrease is related to the ferroelectric polarization switching process. It is more obvious by comparing this curve with the one obtained with the SiO_2 back gate (the inset of Figure 2b). A mobility of $\mu \approx 86.5$ cm^2 V^{-1} s^{-1} is calculated from the polymer gated transfer curve using the method in ref. [8]. Briefly, the mobility was calculated by the expression of $\mu = (dI_{ds}/dV_{bg}) \times (L/(W \cdot \varepsilon_0 \varepsilon_r / d \cdot V_{ds}))$, where $L = 5.0$ μm is the channel length, $W = 6.2$ μm is the channel width, $\varepsilon_r = 10$ is the dielectric constant of P(VDF-TrFE), $d = 300$ nm is the thickness of P(VDF-TrFE) films, and dI_{ds}/dV_{bg} is extracted from left side of the transfer curve in Figure 2b. The measured transfer characteristics exhibit a typical n-type channel FET, showing good agreement with that of a conventional transistor.[8] With the back gate, a mobility of $\mu \approx 24.6$ cm^2 V^{-1} s^{-1} for the few-layer MoS_2 was obtained. The hysteresis behavior is related to the surrounding conditions or the charge transfer from neighboring adsorbates or charge injection into the trap sites on the substrate.[32] The difference in the mobility derived from top or back gates may be associated with the interface nature at the contacts.[33,34] Based on the ferroelectric polymer/MoS_2 structure, we can achieve three different states: P(VDF-TrFE) without polarization (named as the "fresh" state), polarization up state (P_{up}), and polarization down state (P_{down}). The P_{up} and P_{down} states are achieved by poling P(VDF-TrFE) with –40 V and +40 V. During the polarization switching process of ferroelectric polymer, the coercive field is strongly related to the applied voltage and frequency.[35] Additionally, as it is shown in Figure 2b, the MoS_2 channel can be fully accumulation and depletion under ±40 V. A 40V pulse voltage with the pulse width of 2 s is chosen for poling the P(VDF-TrFE) film. The V_{sd}–I_{sd} characteristics (without additional gate voltage and light illumination) of these three states are shown in Figure 2c. In the P_{up} state, I_{sd} is the lowest compared to that of the other two states. This situation means that the depleted state of carriers

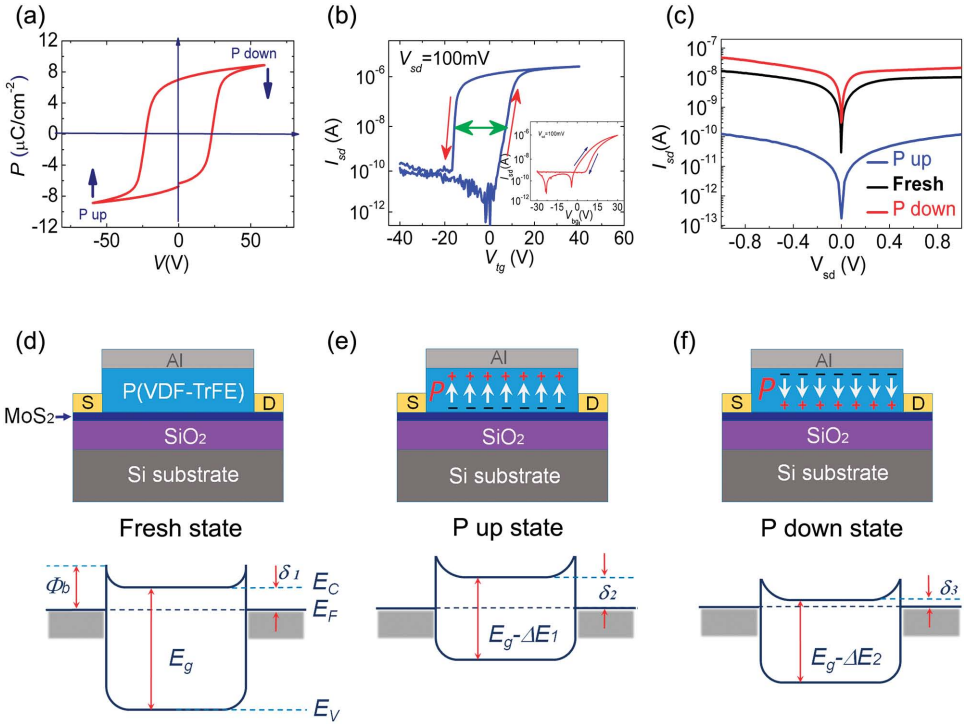

Figure 2. Ferroelectric polarization related electric properties of the P(VDF-TrFE)/MoS_2 hybrid structure. a) The ferroelectric hysteresis loop 300 nm P(VDF-TrFE) film capacitor. It is measured using Sawyer-Tower circuit at 1 Hz applied voltage frequency. b) The transfer curves of triple-layer MoS_2 channel with P(VDF-TrFE) ferroelectric polymer gate on dark state at room temperature. The transfer characteristics of triple-layer MoS_2 with SiO_2 back gate are shown in the inset. c) The V_{sd}–I_{sd} characteristics (at ZERO gate voltage) with three states of ferroelectric layer. The three states are: fresh state (ferroelectric layer without polarization), polarization up ("P_{up}," polarized by a pulse V_g of –40 V), and polarization down ("P_{down}," polarized by a pulse V_g of –40 V) states, respectively. d–f) The cross section structures of the device and equilibrium energy band diagrams of three different ferroelectric polarization states with V_{sd} = 0 V. For the band diagrams of different states, small Schottky barriers at the source and drain electrodes are considered. E_F, E_c, E_V, Φ_B, and E_g are the Fermi level energy, minimum conduction band energy, maximum valence band energy, Schottky barrier height, and band gap of MoS_2, respectively. δ is the height from bottom of conduction band to the Fermi level. δ_1, δ_2, and δ_3 are related to the three states.

in the MoS_2 channel is caused by the electrostatic field derived from the remnant polarization of P(VDF-TrFE). On the other hand, the P_{down} state corresponds to the accumulated states of carriers in the MoS_2 channel. The cross sections of the device structures and equilibrium band diagrams at the different states are shown in Figure 2d–f. For a photodetector, the V_{sd}–I_{sd} represents the dark current level without light illumination.

Next, the photoresponse of the MoS_2 photodetector was measured at a ZERO gate voltage. The photo switching properties (under V_{sd} = 100 mV) at a wavelength of 635 nm with the three states described above are shown in **Figure 3**a. In the fresh state, the signal-to-noise-ratio, photoresponse current (I_{ph}) to dark current (I_{dark}) is very small. In the P_{up} state, a signal-to-noise-ratio of 10^3 is obtained, as can be seen from the photoresponse to pulsed laser illumination curves. In the P_{down} state, I_{ph} cannot be distinguished from the large I_{dark} as the large thermionic and drift/diffusion currents dominate channel current. The results indicate that the electrostatic field produced by the surface charge at the domain surface of P(VDF-TrFE) is strong enough to cause total depletion/accumulation of carriers in the MoS_2 semiconducting channel. The domain direction in the ferroelectric material of a charge insufficiently compensated system can be altered by a depolarization field, which leads to the random distribution of ferroelectric domains and, eventually, to the malfunction of the device. (Indeed, before fabricating the ferroelectric layer, we have characterized the photoresponse properties of back gated MoS_2 photodetector, as shown in Figure S2 (Supporting Information). The performance of the traditional back-gate photodetector is very poor compared to the MoS_2 photodetector with ferroelectric polarization gating.) The photoresponse behavior of our photodetector can be explained by the energy band diagrams as shown in Figure 2d–f. The light illumination results in light absorption and excitation of electron–hole pairs, which can be extracted by applying a drain-source bias. In the P_{down} and fresh states, both photogenerated current and thermionic/tunneling currents contribute device currents as described in ref. [14]. While in P_{up} state, the photogenerated current dominants the channel current, resulting in a high-efficient photocurrent extraction and increased photoresponse, as shown in Figure 3a. Meanwhile, the optothermal effect,[36] which is related to the pyroelectric properties of ferroelectrics, has been excluded in our photodetector. There is no photoresponse for the wavelength of 2 μm light illumination, as it is shown in Figure S10 (Supporting Information). For the following measurement, the ferroelectric polarization in P(VDF-TrFE) was preset at a P_{up} state by a short bias pulse of 40 V on the top gate. The I_{sd}–V_{sd} for different illumination powers at a wavelength of 635 nm is shown in Figure 3b. The I_{sd}–V_{sd} curves, as shown in Figure 3b, are linear and symmetric.

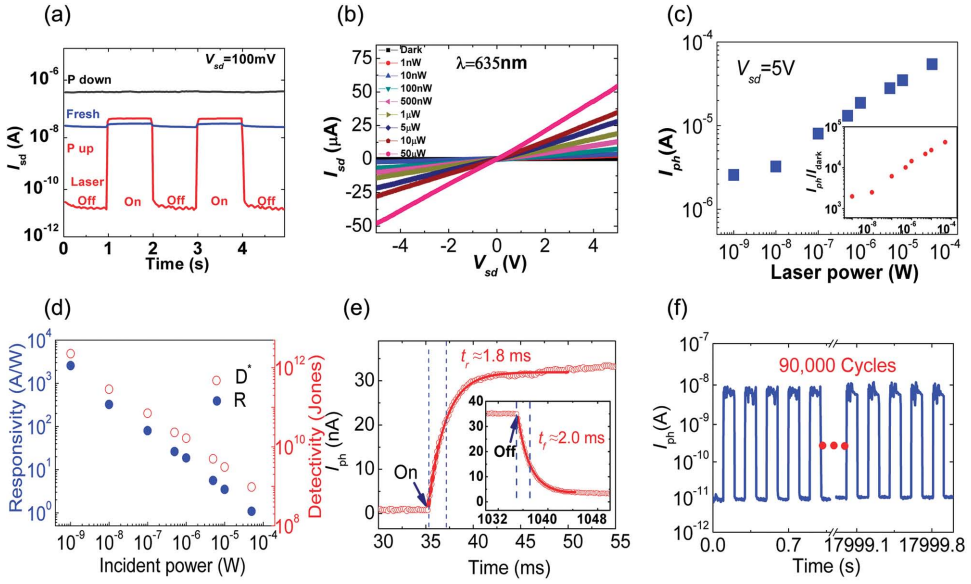

Figure 3. Photoresponse properties of the ferroelectric polarization gating triple-layer MoS_2 photodetector. a) Photoswitching behavior of ferroelectric polarization gating triple-layer MoS_2 photodetector at three states ($\lambda = 635$ nm, $V_{sd} = 100$ mV, $P = 100$ nW). b) Drain–source characteristic of the photodetector in the dark and under different illuminating light powers (1 nW to 50 μW). c) Dependence of photocurrent on illumination powers. The inset is the ratio of photoresponse current to dark current under different illumination powers. d) Photoresponsivity of the MoS_2 phototransistor, showing high sensitivity. The device exhibits a photoresponsivity of 2570 A W^{-1} for an laser power of 1 nW, and the detectivity is up to $\approx 2.2 \times 10^{12}$ Jones. e) The rise and fall of the photocurrent and the fitted data using exponential functions (recorded by $V_{sd} = 100$ mV and $P = 100$ nW). f) Photocurrent response during 90 000 cycles of operation at $V_{sd} = 100$ mV and $P = 100$ nW. The device shows an endurable photoresponse. All of the data are achieved on the same device in the P_{up} state. The difference of I_{ph} in Figure 3a,e,f may be related to the test environment. In addition, the laser power could slightly fluctuate with the humidity of environment.

Figure 3c shows the laser power dependence of I_{ph} of the device with $V_{sd} = 5$ V. The inset in Figure 3c is the ratio of I_{ph} to I_{dark} for light on and light off (dark states) at different illumination powers. It can be seen that the device is very sensitive to illumination power. The responsivity (R) of the photodetector is up to 2570 A W^{-1} and the detectivity is about $\approx 2.2 \times 10^{12}$ Jones (under low illumination power 1 nW). The data are extracted from Figure 3b, where $V_{sd} = 5$ V and $P = 1$ nW, given by $R = I_{ph}/P$, where I_{ph} is the photo current in a detector and P is the illumination power.[37,38] The value of R (2570 A W^{-1}) is larger than previously recorded result ≈880 A W^{-1} (150 pW, $V_{sd} = 8$ V, and $V_g = -70$ V).[8] In addition, the detectivity, assuming that noise from dark current is the major factor, it is given by $D^* = RA^{1/2}/(2eI_{dark})^{1/2}$, where R is the responsivity, A is the area of the detector, e is the unit charge, and I_{dark} is the dark current.[39] The maximum detectivity $\approx 2.2 \times 10^{12}$ Jones has been achieved, which is higher than that of detectors based on 2D materials. As shown in Figure 3d, the high detectivity and responsivity decrease dramatically with the increasing signal power. This decreasing can be explained that trap states present either in MoS_2 or at the interface between MoS_2 and P(VDF-TrFE) layer.[40] Note that, if a highly transparent electrode (for example graphene, Ag nanowire) is chosen, a higher responsivity can be expected. Currently, the transmittance of the available semitransparent Al electrode is only 30% for our device. It suggests that a flawless device fabrication is needed for superior performance in the future.

In addition to the superior sensitivity and good photoresponsivity, we conducted time-resolved photoresponse experiments by periodically turning the illuminating laser on and off at a frequency of 0.5 Hz and recording the response signal with a high speed oscilloscope (as shown in Figure S3 in the Supporting Information). Figure 3e shows a complete on/off cycle in which the photocurrent exhibits rapid rise/fall and reaches a steady saturation. The rising and falling edges of the response current are perfectly fitted by a single exponential function. The rise (τ_r) and decay (τ_f) times of the photocurrent, are ≈1.8 ms and ≈2 ms, respectively, which is relatively fast for state-of-the-art 2D photoconductive photodetectors. In our case, the improvement of response time may result from the interface of P(VDF-TrFE) and MoS_2, the surface trap state of MoS_2 may be encapsulated or passivated by the fluorine or hydrogen atoms from polarized P(VDF-TrFE). Furthermore, the signals recorded by the oscilloscope remain nearly unchanged after 90 000 cycles of operation (as shown in Figure 3f), pointing to the excellent stability and reliability of the photodetectors. The stability of the photo-switching behavior is related to the ferroelectric polarization stability of the P(VDF-TrFE) top gate[41,42] and the reliability of the P(VDF-TrFE)-passivated MoS_2 channel.

All the prominent properties of our photodetector benefit from the ferroelectric-polarization-induced ultrahigh electrostatic field of the P(VDF-TrFE). The local electric field at the interface between P(VDF-TrFE) and MoS_2 layers can be estimated from $\sigma = \varepsilon\varepsilon_0 E$, where σ is the charge density at the surface of P(VDF-TrFE) film, which is related to the remnant polarization (P_r) of the ferroelectric materials,[27] ε is the dielectric constant of material (the dielectric constant of MoS_2 is ≈4–6,[43,44] ε_0 is the vacuum permittivity, E is the electric field strength, and P_r is ≈7.0 μC cm^{-2} calibrated from Figure 2a. The calculated electric field applied to the triple-layer MoS_2 is

about 0.5×10^9 V m^{-1}. It is very difficult to obtain such an ultra-high electric field for conventional FETs as described by several research groups.[27,45–47]

The typical photoresponse spectra of an MoS_2 photodetector is from visible to near-infrared (0.85 μm) as the band gap of MoS_2 ranges from 1.2 eV to 1.8 eV. As reported by Oriol Lopez-Sanchez et al., photoresponse is negligible at wavelengths longer than 680 nm (corresponding to one photon energy 1.8 eV) for monolayer MoS_2.[14] For triple-layer MoS_2, the broad absorption tail corresponding to the indirect band transition extends to near 0.85 μm, which is in good agreement with the theoretical prediction.[17] In this work, we also characterized the photoresponse properties of fresh state MoS_2 photodetector, where the response wavelength ends at ≈900 nm (as shown in Figure S4 in the Supporting Information). A wider spectral response for a photodetector is important and meaningful. Therefore, the response of the detector to light with long wavelength was investigated. The photoresponse of the detector to laser illumination with different wavelengths is shown in **Figure 4**a. Surprisingly, it is found that there is still appreciable optical current response to light with wavelength up to 1.55 μm. For the first time, our work broadens the detection of an MoS_2 photodetector from 0.85 to 1.55 μm.

To confirm the effect of the electric field polarization on the band structure of few-layer MoS_2, we carried out micro-photoluminescence (PL) measurements on the fresh (ferroelectric domain random) and poled (domain aligned) samples (in Figure 4b). The PL emission for the pole sample is red-shifted compared to that of the fresh sample, In addition, the PL emission intensity is also increased after the cover of poled P(VDF-TrFE). This PL emission intensity increasing may be related to the electric field modifying the band structure of the MoS_2 and in turn increasing the density of states of the carriers. With the increase in the carrier population, the radiative recombination of carriers increases, which leads to an increase in PL intensity.[48,49] Similarly, the band structure of MoS_2 can be tuned by the external strain and confirmed by PL spectrum.[48–51] Note that an optical band gap measured by PL is different from the band gap of electron transport due to the exciton binding energy. It has been theoretically predicted that the energy gap of the bilayer MoS_2 can be tuned by the external electric field.[52,53] The change in the band gap in triple-layer MoS_2 under external electric fields applied perpendicular to the layers was also calculated using the density functional theory. The band structure of triple-layer MoS_2 as a function of applied different external electric field is shown in Figure 4c–e. For example, a 0.40 V nm^{-1} of electric field strength can reduce the band gap from 1.09 to 0.71 eV (details of the calculation are shown in the Supporting Information). The indirect band gap is reduced with an increase of the applied electric field, and the relationship between E_g and electric field is linear (as shown in Figure S6 in the Supporting Information). Additionally, the electrostatic fields from the ferroelectrics may induce defects in MoS_2. Such defects in transition metal dichalcogenides could also be one of the possible reasons for the PL spectrum variation.[54]

Further studies are needed to clarify the fundamental physics principles of the ferroelectric polarization tuning for the band gap of few-layer MoS_2. Nevertheless, the ferroelectric/MoS_2 hybrid structure photodetector shows an outstanding performance for detection. Similar electric and photoresponse

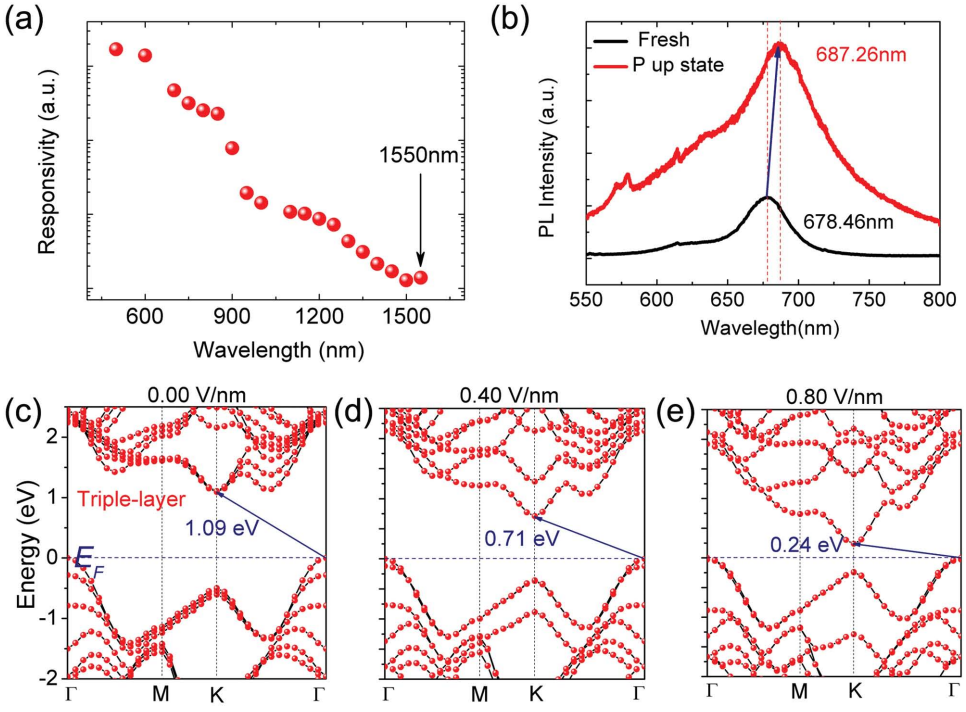

Figure 4. Infrared photoresponse of ferroelectric polarization gating few-layer MoS_2 photodetector beyond its intrinsic band gap. a) Photoresponsitivity of a similar polarization-gating triple layer MoS_2 photodetector as a function of light wavelength from 500 nm to 1550 nm at V_{sd} = 1 V, P = 100 μW under P_{up} state. b) Comparison photoluminescence spectrum of fresh and polarization gating triple-layer MoS_2. c–e) The band structures evolution of triple-layer MoS_2 under different external electric field (0.0, 0.4, and 0.8 V nm^{-1}) by first-principles DFT calculations.

properties have also been achieved on the same structure with four-layer MoS_2 photodetector (as shown in Figures S7 and S8 in the Supporting Information). Our photodetector shows a high sensitivity under weak illumination, such as fluorescent lamp, demonstrating that the few-layer MoS_2 is very promising for a visible to near-infrared digital camera.

In summary, we have fabricated a ferroelectric polymer film gated triple-layer MoS_2. The MoS_2 device exhibited outstanding photodetection capabilities compared to traditional MoS_2 FET photodetectors. The device exhibits a maximum attainable photoresponsivity of 2570 A W^{-1}, and high detectivity of 2.2×10^{12} Jones, which are record values compared to the previous reports on MoS_2 and other 2D material photodetector. In addition, the broad spectral regions detection, stable and fast photoresponse of the detector are also superior to recently reported MoS_2 photodetectors. The infrared (0.85–1.55 μm) photoresponse of the ferroelectric polarization gating MoS_2 photodetector suggests that such an MoS_2 photodetector is very promising for use in optical communications. The energy gap engineering of a 2D material system combined with an ultrahigh ferroelectric-polarization-induced electrostatic field is an attractive research area for next-generation high performance 2D electronic/optoelectronic devices. There are many fruitful and fundamental physics issues in ferroelectric/photoelectric 2D material hybrid systems to be explored in future studies.

All measurements were performed under ambient conditions. Triple layers of MoS_2 were exfoliated from commercially available crystals of molybdenite (SPI Supplies brand Moly Disulfide) using the Scotch-tape micromechanical cleavage technique pioneered for the production of graphene. Triple layers of MoS_2 were deposited on a ≈285 nm thick SiO_2 dielectric layer on top of a highly-doped p-type Si wafer (resistivity $< 5 \times 10^{-3}$ Ω cm). Electrical contacts were patterned on top of MoS_2 flakes using a conventional lift-off technique. Cr (5 nm) and Au (50 nm) electrodes were deposited by thermal evaporation at room temperature. The device was then annealed at 200 °C in a vacuum tube furnace for 2 h (100 sccm Ar) to remove resist residue and to decrease contact resistance. The P(VDF-TrFE) (70:30 mol%) ferroelectric polymer power was dissolved in the diethyl carbonate with 2.5%wt firstly. Then the P(VDF-TrFE) films were prepared by spin coating on the top of the MoS_2. After that, the P(VDF-TrFE) films were annealed at 135 °C for four hours for improving their crystallinity. Finally, ultrathin aluminum films were deposited by thermal evaporation and patterned by photolithography as the top gate semitransparent electrodes.

We performed the electrical and optoelectrical characterization of our device at room temperature using a Lake Shore probe station and Agilent semiconductor parameter analyzer.

In this work, electrical measurements were carried out using an Agilent B2902A, Signal Recovery current preamplifier, lock-in amplifier Signal Recovery 7270 and a current preamplifier Signal Recovery 5182 on the Lake Shore probe station. The photoresponse to laser excitation used a focused λ = 500–1550 nm laser beam. A monochrometer was used for wavelength-dependent measurements of the photocurrent. The Raman spectra and PL spectra were acquired by the Lab Ram HR800 from HORIBA (excitation wavelength 532 nm, power 2 mW, spot size 2–3 μm). Time-resolved photoresponse were achieved by the high-speed Tektronix MDO3014 Oscilloscope.

Supporting Information

Supporting Information is available from the Wiley Online Library or from the author.

Acknowledgements

This work was partially supported by the Ten Thousand Talents Program for Young Talents, Major State Basic Research Development Program (Grant Nos. 2013CB922302 and 2014CB921600), Natural Science Foundation of China (Grant Nos. 11374320, 11322441, 61440063 and 61574152), and Fund of Shanghai Science and Technology Foundation (Grant No. 14JC1406400). X.W. and P.W. contributed equally to this work. J.W. and W.H. conceived and supervised the research. X.W. and J.W. fabricated the devices. X.W. and P.W. performed the measurements. X.Z. carried out the calculated part. J.W. and W.H. wrote the paper. All authors discussed the results and revised the manuscript. The authors declare no competing financial interests.

Received: July 10, 2015
Revised: August 12, 2015
Published online: September 16, 2015

[1] K. S. Novoselov, A. K. Geim, S. V. Morozov, D. Jiang, Y. Zhang, S. V. Dubonos, I. V. Grigorieva, A. A. Firsov, *Science* **2004**, *306*, 666.
[2] K. S. Novoselov, D. Jiang, F. Schedin, T. J. Booth, V. V. Khotkevich, S. V. Morozov, A. K. Geim, *Proc. Natl. Acad. Sci. USA* **2005**, *102*, 10451.
[3] N. M. Gabor, J. C. W. Song, Q. Ma, N. L. Nair, T. Taychatanapat, K. Watanabe, T. Taniguchi, L. S. Levitov, P. Jarillo-Herrero, *Science* **2011**, *334*, 648.
[4] F. Xia, T. Mueller, Y. Lin, A. Valdes-Garcia, P. Avouris, *Nat. Nanotechnol.* **2009**, *4*, 839.
[5] J. R. Williams, L. DiCarlo, C. M. Marcus, *Science* **2007**, *317*, 638.
[6] H. Yang, J. Heo, S. Park, H. J. Song, D. H. Seo, K. Byun, P. Kim, I. Yoo, H. Chung, K. Kim, *Science* **2012**, *336*, 1140.
[7] L. Britnell, R. V. Gorbachev, R. Jalil, B. D. Belle, F. Schedin, A. Mishchenko, T. Georgiou, M. I. Katsnelson, L. Eaves, S. V. Morozov, N. M. R. Peres, J. Leist, A. K. Geim, K. S. Novoselov, L. A. Ponomarenko, *Science* **2012**, *335*, 947.
[8] B. Radisavljevic, A. Radenovic, J. Brivio, V. Giacometti, A. Kis, *Nat. Nanotechnol.* **2011**, *6*, 147.
[9] A. N. Grigorenko, M. Polini, K. S. Novoselov, *Nat. Photon.* **2012**, *6*, 749.
[10] C. Lee, G. Lee, A. M. Zande, W. Chen, Y. Li, M. Han, X. Cui, G. Arefe, C. Nuckolls, T. F. Heinz, J. Guo, J. Hone, P. Kim, *Nat. Nanotechnol.* **2014**, *9*, 676.
[11] H. Yuan, X. Liu, F. Afshinmanesh, W. Li, G. Xu, J. Sun, B. Lian, A. G. Curto, G. Ye, Y. Hikita, Z. Shen, S. Zhang, X. Chen, M. Brongersma, H. Y. Hwang, Y. Cui, *Nat. Nanotechnol.* **2015,** *10*, 707.
[12] F. H. L. Koppens, T. Mueller, Ph. Avouris, A. C. Ferrari, M. S. Vitiello, M. Polini, *Nat. Nanotechnol.* **2014**, *9*, 780.
[13] B. W. H. Baugher, H. O. H. Churchill, Y. Yang, P. Jarillo-Herrero, *Nat. Nanotechnol.* **2014**, *9*, 262.
[14] O. Lopez-Sanchez, D. Lembke, M. Kayci, A. Radenovic, A. Kis, *Nat. Nanotechnol.* **2013**, *8*, 497.
[15] Z. Yin, H. Li, H. Li, L. Jiang, Y. Shi, Y. Sun, G. Lu, Q. Zhang, X. Chen, H. Zhang, *ACS Nano* **2012**, *6*, 74.
[16] H. S. Lee, S. Min, Y. Chang, M. K. Park, T. Nam, H. Kim, J. H. Kim, S. Ryu, S. Im, *Nano Lett.* **2012**, *12*, 3695.

[17] W. Choi, M. Y. Cho, A. Konar, J. H. Lee, G. Cha, S. H. Hong, S. Kim, J. Kim, D. Jena, J. Joo, S. Kim, *Adv. Mater.* **2012**, *24*, 5832.
[18] K. F. Mak, C. Lee, J. Hone, J. Shan, T. F. Heinz, *Phys. Rev. Lett.* **2010**, *105*, 136805.
[19] C. Lee, H. Yan, L. E. Brus, T. F. Heinz, J. Hone, S. Ryu, *ACS Nano* **2010**, *4*, 2695.
[20] R. Ganatra, Q. Zhang, *ACS Nano* **2014**, *8*, 4074.
[21] H. Liu, A. T. Neal, P. D. Ye, *ACS Nano* **2012**, *6*, 8563.
[22] S. Bertolazzi, D. Krasnozhon, A. Kis, *ACS Nano* **2013**, *7*, 3246.
[23] H. Qiu, L. Pan, Z. Yao, J. Li, Y. Shi, X. Wang, *Appl. Phys. Lett.* **2012**, *100*, 123104.
[24] A. M. Ionescu, H. Riel, *Nature* **2011**, *479*, 329.
[25] Y. Ouyang, J. Guo, *Appl. Phys. Lett.* **2006**, *89*, 183122.
[26] Y. Zheng, G. Ni, C. Toh, C. Tan, K. Yao, B. Ozyilmaz, *Phys. Rev. Lett.* **2010**, *105*, 166602.
[27] R. C. G. Naber, C. Tanase, P. W. M. Blom, G. H. Gelinck, A. W. Marsman, F. J. Touwslager, S. Setayesh, D. M. Deleeuw, *Nat. Mater.* **2005**, *4*, 243.
[28] C. Baeumer, S. P. Rogers, R. Xu, L. W. Martin, M. Shim, *Nano Lett.* **2013**, *13*, 1693.
[29] H. S. Lee, S. Min, M. K. Park, Y. T. Lee, P. J. Jeon, J. H. Kim, S. Ryu, S. Im, *Small* **2012**, *8*, 3111.
[30] C. Baeumer, D. Saldana-Greco, J. M. P. Martirez, A. M. Rappe, M. Shim, L. W. Martin, *Nat. Commun.* **2015**, *6*, 6136.
[31] A. Nguyen, P. Sharma, T. Scott, E. Preciado, V. Klee, D. Sun, I. Lu, D. Barroso, S. Kim, V. Y. Shur, A. R. Akhmatkhanov, A. Gruverman, L. Bartels, P. A. Dowben, *Nano Lett.* **2015**, *15*, 3364.
[32] H. Wang, Y. Wu, C. Cong, J. Shang, T. Yu, *ACS Nano* **2010**, *4*, 7221.
[33] D. Jena, A. Konar, *Phys. Rev. Lett.* **2007**, *98*, 136805.
[34] V. A. Fonoberov, A. A. Balandin, *Nano Lett.* **2006**, *6*, 2442.
[35] B. B. Tian, Z. H. Chen, A. Q. Jiang, X. L. Zhao, B. L. Liu, J. L. Wang, L. Han, Sh. Sun, J. L. Sun, X. J. Meng, J. H. Chu, *Appl. Phys. Lett.* **2013**, *103*, 042909.
[36] C. Y. Hsieh, Y. T. Chen, W. J. Tan, Y. F. Chen, W. Y. Shih, W. H. Shih, *Appl. Phys. Lett.* **2012**, *100*, 113507.
[37] G. Konstantatos, E. H. Sergeant, *Nat. Nanotechnol.* **2010**, *5*, 391.
[38] Y. Guo, G. Yu, Y. Liu, *Adv. Mater.* **2010**, *22*, 4427.
[39] Y. Hu, J. Zhou, P. Yeh, Z. Li, T. Wei, Z. L. Wang, *Adv. Mater.* **2010**, *22*, 3327.
[40] S. Ghatak, A. N. Pal, A. Ghosh, *ACS Nano* **2011**, *5*, 7707.
[41] W. Y. Kim, D. Y. Ka, B. Cho, S. Y. Kim, Y. S. Lee, H. C. Lee, *IEEE Electron Device Lett.* **2009**, *30*, 822.
[42] T. J. Reece, A. Gerber, H. Kohlstedt, S. Ducharme, *J. Appl. Phys.* **2010**, *108*, 024109.
[43] X. Chen, Z. Wu, S. Xu, L. Wang, R. Huang, Y. Han, W. Ye, W. Xiong, T. Han, G. Long, Y. Wang, Y. He, Y. Cai, P. Sheng, N. Wang, *Nat. Commun.* **2015**, *6*, 6088.
[44] E. J. G. Santos, E. Kaxiras, *ACS Nano* **2013**, *7*, 10741.
[45] R. Gysel, I. Stolichnov, A. K. Tagantsev, S. W. E. Riester, N. Setter, G. A. Salvatore, D. Bouvet, A. M. Ionescu, *Appl. Phys. Lett.* **2009**, *94*, 263507.
[46] S. L. Miller, P. J. McWhorter, *J. Appl. Phys.* **1992**, *72*, 5999.
[47] J. S. Miao, W. D. Hu, Y. L. Jing, W. J. Luo, L. Liao, A. L. Pan, S. W. Wu, J. X. Cheng, X. S. Chen, W. Lu, *Small* **2015**, *11*, 2392.
[48] Y. Y. Hui, X. Liu, W. Jie, N. Y. Chan, J. Hao, Y. Hsu, L. Li, W. Guo, S. P. Lau, *ACS Nano* **2013**, *7*, 7126.
[49] S. Mouri, Y. Miyauchi, K. Matsuda, *Nano Lett.* **2013**, *13*, 5994.
[50] H. J. Conley, B. Wang, J. I. Ziegler, R. F. Haglund Jr., S. T. Pantelides, K. I. Bolotin, *Nano Lett.* **2013**, *13*, 3626.
[51] A. Castellanos-Gomez, R. Roldan, E. Cappelluti, M. Buscema, F. Guinea, H. S. J. van der Zant, G. A. Steele, *Nano Lett.* **2013**, *13*, 5361.
[52] A. Ramasubramaniam, D. Naveh, E. Towe, *Phys. Rev. B* **2011**, *84*, 205325.
[53] N. Zibouche, P. Philipsen, A. Kuc, T. Heine, *Phys. Rev. B* **2014**, *90*, 125440.
[54] P. K. Chow, R. J. Gedrim, J. Gao, T. M. Lu, B. Yu, H. Terrones, N. Koratkar, *ACS Nano* **2015**, *9*, 1520.